

Evidence of strong radiation reaction in the field of an ultra-intense laser

K. Poder,¹ M. Tamburini,² G. Sarri*,^{3,4} A. Di Piazza,² S. Kuschel,^{5,6}
C. D. Baird,⁷ K. Behm,⁸ S. Bohlen,⁹ J. M. Cole,¹⁰ M. Duff,¹¹ E. Gerstmayr,¹⁰
C. H. Keitel,² K. Krushelnick,⁸ S. P. D. Mangles,¹⁰ P. McKenna,¹¹
C. D. Murphy,⁷ Z. Najmudin,¹⁰ C. P. Ridgers,⁷ G. M. Samarin,³
D. Symes,¹² A. G. R. Thomas,^{8,13} J. Warwick,³ and M. Zepf^{3,5,6}

¹*The John Adams Institute for Accelerator Science,
Blackett Laboratory, Imperial College London, London SW7 2AZ, UK*

²*Max-Planck-Institut für Kernphysik,
Saupfercheckweg 1, D-69117 Heidelberg, Germany*

³*School of Mathematics and Physics, Queen's University Belfast,
University Road, Belfast BT7 1NN, UK*

⁴*corresponding author*

⁵*Helmholtz Institute Jena, Fröbelstieg 3, 07743 Jena, Germany*

⁶*Institut für Optik und Quantenelektronik,
Friedrich-Schiller-Universität Jena, Max-Wien-Platz 1, 07743 Jena, Germany*

⁷*Department of Physics, University of York,
Heslington, York, YO10 5DD, United Kingdom*

⁸*Center for Ultrafast Optical Science, University of Michigan,
Ann Arbor, Michigan 48109-2099, USA*

⁹*Deutsches Elektronen Synchrotron DESY, Hamburg 22607, Germany*

¹⁰*The John Adams Institute for Accelerator Science,
Blackett Laboratory, Imperial College London, London SW72BZ, UK*

¹¹*Department of Physics, SUPA, University of Strathclyde, Glasgow, G4 0NG, UK*

¹²*Central Laser Facility, Rutherford Appleton Laboratory,
Didcot, Oxfordshire OX11 0QX, UK*

¹³*Lancaster University, Lancaster LA1 4YB, United Kingdom*

(Dated: April 28, 2024)

The description of the dynamics of an electron in an external electromagnetic field of arbitrary intensity is one of the most fundamental outstanding problems in electrodynamics. Remarkably, to date, there is no unanimously accepted theoretical solution for ultra-high intensities and little or no experimental data. The basic challenge is the inclusion of the self-interaction of the electron with the field emitted by the electron itself – the so-called radiation reaction (RR)[1, 2]. At low field-strengths, where RR is negligible, the equation of motion is the well-known Lorentz equation [1]. At higher field-strengths but still in the classical limit the Landau-Lifshitz equation is the most widely accepted solution. For the strongest fields a full quantum description is required and this is currently the subject of active research [3–6]. We report on the first experimental evidence of strong radiation reaction during the interaction of a relativistic electron beam with a high-intensity laser field. Our results pave the way for systematic studies into the precision measurements of one of the most fundamental effects of electrodynamics.

In the realm of classical electrodynamics, the problem of radiation reaction (RR) is satisfactorily described by the Landau-Lifshitz equation (LL) [1], which has been theoretically demonstrated to be the self-consistent classical equation of motion for a charged particle [1, 7]. However, when the electron experiences an extremely intense field the LL equation can no longer be assumed valid [2]. In such fields purely quantum effects, such as the stochastic nature of photon emission [4], a hard cut-off in the maximum energy of the emitted photons [8], and pair production [9] become sizable and must be taken into account.

Besides the intrinsic fundamental interest in investigating this regime in laboratory experiments, RR is invoked to explain the radiative properties of powerful astrophysical objects, such as pulsars and quasars [10]. A detailed characterisation of RR is also important for the description of high-field experiments using the next generation of multi-petawatt laser facilities, such as the Extreme Light Infrastructure [11], Apollon [12], Vulcan 20PW [13], XCELS [14] where focussed intensities exceeding 10^{23} W/cm² are expected. The data presented here paves the way for detailed experimental studies of RR and high-field quantum electrodynamics.

The LL equation is obtained assuming that the electromagnetic field in the rest frame of

the electron is much smaller than the classical critical field $F_0 = m_e^2 c^4 / e^3 \approx 1.8 \times 10^{20}$ V/m [1] and constant over distances of the order of the classical electron radius $r_0 = e^2 / m_e c^2 \approx 2.8 \times 10^{-15}$ m. These conditions are automatically satisfied in classical electrodynamics since quantum effects are negligible as long as the rest frame fields are much smaller than the critical field of Quantum Electrodynamics (QED) $F_{cr} = \alpha F_0 \approx 1.3 \times 10^{18}$ V/m $\ll F_0$ [8] and remain constant over distances of the order of the reduced Compton wavelength $\lambda_C = r_0 / \alpha \approx 3.9 \times 10^{-13}$ m $\gg r_0$ ($\alpha \approx 1/137$ is the fine structure constant). Even for GeV electrons with Lorentz factor $\gamma_e \gtrsim 2000$, the micron-scale wavelength of typical high-power laser systems ($\lambda_L \approx 0.8 - 1 \mu\text{m}$) implies that the only relevant condition on classicality is on the laser field amplitude F_L , which can be expressed by stating that the quantum parameter $\chi \approx (1 - \cos \theta) \gamma_e F_L / F_{cr}$ has to be much smaller than unity. Here θ is the angle between the laser propagation direction and the electron momentum. Thus the validity of the LL approach can be expected to break down when quantum effects on the electron's motion become important, i.e., at $\chi \gtrsim 1$. In the intense fields that can be created by modern-day lasers, the possibility of multi-photon absorption within a single photon formation length depends on the dimensionless amplitude $a_0 = e F_L \lambda_L / 2\pi m_e c^2$, which roughly relates to the number of laser photons absorbed per formation length [9]. Available lasers allow now for experimental investigations of the strong-field regime where $a_0 \gg 1$.

To date, only one laser-based experimental campaign has reached a non-negligible value of $\chi \approx 0.2$ [15, 16]. Whilst these experiments gave evidence of non-linearities in Compton scattering ($a_0 < 1$) [15] and generation of electron-positron pairs [16], no measurements were performed to assess the level of RR in the scattered electron beam.

The multi-GeV electrons available at accelerator laboratories world-wide would provide an excellent basis for RR studies in the non-linear and quantum regime, but are rarely available concurrently with ultra-intense lasers. The development of compact, laser-driven wakefield accelerators (LWFA) [17] provides a well-suited alternative, since it allows GeV electron beams to be generated directly at high power laboratories capable of achieving field strengths of $a_0 \gg 1$. The plausibility of such an experimental approach is evidenced by the observation of non-linearities in Compton scattering in previous experimental campaigns [18–20], motivating the study reported here.

In this experiment we obtained a maximum quantum parameter $\chi \approx 0.2$ by interacting a multi-GeV electron beam (maximum Lorentz factor $\gamma_e \approx 4 \times 10^3$) [22] with a high intensity

laser pulse ($\lambda_L = 0.8 \mu\text{m}$ and intensity $I_L \approx 2 \times 10^{20} \text{ W/cm}^2$ or $a_0 \approx 10$). Under these circumstances the energy loss due to RR becomes substantial (up to 30%) and requires RR to be included in any model of the electron trajectory. To the best of our knowledge, this is the first direct experimental evidence of strong radiation reaction of an electron in an intense laser field.

The experimental set-up is shown schematically in Fig. 1a. One of the twin laser beams of the Astra Gemini laser system (Driver Laser in Fig. 1a), was focussed at the entrance of a helium-filled gas-cell producing an electron beam via LWFA with an energy spectrum extending to approximately 2 GeV. The electron source size (FWHM diameter) is estimated to be $D_e \leq 1 \mu\text{m}$ and the energy dependent beam divergence was measured to be in the range of 1 mrad for electrons exceeding 1 GeV.

The second laser beam (Scattering Laser in Fig. 1a) was focussed, in a counter-propagating geometry, 1 cm downstream from the end of the gas-cell, with an intensity distribution as shown in Fig. 1b. At this point the GeV electron beam had expanded to approximately 10 μm diameter. Due to the inherent lag of the laser-accelerated electron beam in respect to the driver laser, the electrons are estimated to reach the focal spot of the scattering laser with a delay of the order of 64 fs (see Methods for details). Numerical calculations indicate that, at this time, the laser has defocussed to a rather flat intensity distribution with a peak dimensionless amplitude of $a_0 \simeq 12$ and a full width half maximum of 7 μm (see Fig. 1c). After the interaction with the laser field, the electrons were spectrally resolved by a magnetic spectrometer whereas the Compton-generated γ -ray beam was detected by a caesium-iodide scintillator. Full details of the experimental configuration are given in the Methods section.

The LWFA generating GeV level electron beams [21, 22] was run in a regime of good stability with the spectral shape of the electron beam being a stable and reproducible function of the input laser energy (frames b-d in Fig. 2). In Fig. 2, we show the linear correlation between the energy of the laser driving the wakefield and the cut-off energy of the accelerated electron beam. This allows the effect of RR to be determined by comparing spectra with the scattering laser off with those obtained with the scattering laser on with the same driver laser energy. The analysis was based on spectra normalised by dividing the measured spectrum by the overall number of electrons with energy exceeding 350 MeV, to eliminate shot-to-shot fluctuations in the total electron number (see Methods). These shot-to-shot

fluctuations were included in the subsequent theoretical analysis performing simulations for a range of input spectra shown as a band in Figs. 2b-d.

The intrinsic shot-to-shot pointing fluctuations of LWFA beams [23] results in a statistical fluctuation of the spatial overlap of the laser spot with the electron beam (10 – 15 μm diameter at the interaction point). To discern between shots of poor and good overlap we use the energy contained in the Compton-scattered γ -ray beam during the interaction. The number of photons scales as $N_{ph} \propto \int a_0 N_e(a_0) da_0$, with $N_e(a_0)$ the number of electrons interacting with a field of amplitude a_0 [24]. Fig. 3a shows the correlation between the energy loss in the electron beam and the energy observed in a caesium iodide γ -ray detector placed four metres downstream of the interaction, validating this approach. Shots with a weak signal on the caesium iodide detector (poor overlap) show virtually no change in the spectrum of the scattered electrons (see Fig. 3b) whereas the strongest spectral modification is seen for shots with good overlap and strongest γ -ray signal (Fig. 3d).

We will therefore focus our attention only on shots where the caesium iodide detector indicates best overlap between the high-energy component of the electron beam and the scattering laser focus (region d in Fig. 3a). A comparison between the reference electron spectrum (scattering laser off) and a perturbed electron spectrum (scattering laser on) for conditions of best overlap is shown in Fig. 3d. The corresponding reference electron spectra and uncertainty band is shown in Fig. 2b and exhibit a spectral profile that decreases with energy up to 2 GeV, with a clear local peak at approximately 1.2 GeV. The electron spectrum perturbed by the interaction with the scattering laser beam (red line in Fig. 3d) shows significant depletion of high-energy electrons, with virtually no electrons with energy exceeding 1.6 GeV. Moreover, the local maximum in the spectrum is now shifted down to an energy of approximately 1 GeV and there is clear accumulation of electrons for lower energies, suggesting a net energy loss for the highest energy electrons of the order of 30 - 40%.

The overall magnitude of this significant energy loss is consistent with a classical estimate based on the LL equation. For our experiments, the analytical solution of this equation, assuming a plane wave with a Gaussian temporal profile, provides [25]:

$$\frac{\Delta\gamma_e}{\gamma_e} \approx \frac{\sqrt{\pi/\log 2\tau_0 t_L \omega_L^2 \gamma_e a_0^2}/2}{1 + \sqrt{\pi/\log 2\tau_0 t_L \omega_L^2 \gamma_e a_0^2}/2}, \quad (1)$$

with $\tau_0 = 2r_0/3c \approx 6.3 \times 10^{-24}$ s, $t_L = 42 \pm 3$ fs the laser duration, and $\omega_L = 2.4 \times 10^{15}$ rad/s the laser carrier frequency (see also Ref. [26]). For $\gamma_e = 4000$ and $a_0 = 10$, the LL equation predicts an energy loss of about 40%, consistent with the experimental findings.

A quantitative comparison between the experimental data and the theoretical models requires a detailed comparison of the measured spectra with those predicted by different models using the reference spectra as input. Fig. 4 shows the normalised experimental spectra of the scattered electrons in conditions of best overlap and the corresponding theoretical spectra obtained by simulating the effect of the scattering laser on reference spectrum using different models and both a multi-particle code and a Particle-In-Cell (PIC) code. Both multi-particle and PIC approaches are described in detail in the Methods section. The error bands of the multi-particle code correspond to the uncertainties in the reference electron spectra as well as uncertainties in the intensity of the scattering laser (see Methods).

The models implemented within the multi-particle approach correspond to different degrees of approximation. The green band in Fig. 4a depicts the results of a model routinely used in accelerators [27]. In this case, the electron trajectory is calculated via the Lorentz force and the electron energy loss is only accounted for by subtracting the total energy emitted by each electron after the laser-electron interaction. In this regime, RR is thus neglected during the passage of the electron through the laser field. This approach fails to describe the data, greatly overestimating the energy loss and thus providing a strong indication that a proper treatment of RR is required to calculate the electron trajectories correctly. Fig. 4b depicts the results from the LL equation, which is able to reproduce the characteristic spectral shape of the scattered electrons and exhibits a much closer agreement with the experimental data overall. Despite the rather large uncertainty in the data, it is interesting to note that there is a first indication of the LL equation slightly overestimating the energy loss experienced by the electron beam, with the experimental data better reproduced for a laser amplitude at the lower bound of the experimental uncertainty. Even though the experimental data does not allow us to draw a definite conclusion in this regard, a slight overestimate of the energy loss is to be expected due to the non-negligible value of the quantum parameter χ in this experiment. This overestimate is due to the fact that the LL equation does not include the hard cut-off in the maximum energy of the emitted photons predicted by quantum physics (see, for instance, Ref. [9]) and, therefore, overestimates the total energy of the emitted photons.

This effect can be theoretically included in the model by weighting the LL equation with a function $g(\chi)$, which arises from the ratio of purely quantum and classical spectra of the emitted photon [28]. The inclusion of this weighting function results in a “semi-classical” treatment that, while still assuming continuous photon emission, includes a hard cut-off in the photon spectrum. A comparison between the predictions of this model and the experimental results is shown in Fig. 4c. The improved agreement of the semiclassical LL model compared to the unmodified LL provides an indication of the onset of quantum effects under the conditions of the experiment.

Finally, a comparison between the experimentally measured spectrum of the scattered electrons and numerical calculations based on a multi-particle QED code (green curve) is shown in Fig. 4d. This model is, within the uncertainties of the experiment, able to reproduce the general features of the experimental data. However, there is a clear indication of a non-negligible mismatch, especially in the shape of the spectrum as the quantum model does not show a knee in the final electron spectrum. In order to rule out collective effects in the electron beam, matching 3-dimensional PIC simulations using the code EPOCH [29] have also been carried out (see Methods). Indeed, the PIC and the multi-particle QED model yield very similar results showing that collective effects are negligible in our experimental conditions (see Fig. 4.d). In addition, we stress that we have performed an extensive parametric scan on the laser amplitude and on the position of the interaction point without being able, in particular, to reproduce the knee via the quantum model. One possible source of mismatch arises from the fact that the so-called local-constant-crossed field approximation [9], a common approximation adopted in this class of calculations which assumes $a_0 \gg 1$, may not be accurate at the moderate a_0 achieved in the experiment. In this respect, this might be a first hint on the failure of the local-constant-crossed field approximation [30]. Other possible reasons for the discrepancy include the experimental limitations regarding knowledge of quantities such as the phase content and longitudinal distribution of the laser beam and the exact laser and electron beam transverse distributions at the collision.

While not shown here, our modelling is also capable of reproducing the perturbed spectra at reduced levels of radiation reaction shown in region c of Fig. 3a (related spectra in Fig. 3c) by taking into account the shot-to-shot fluctuations in spatial overlap between the scattering laser and the electron beam.

In conclusion, we report on the first experimental detection of strong radiation reaction in an all-optical experiment. The experimental data give clear evidence of significant energy loss ($> 30\%$) of ultra-relativistic electrons during its interaction with an ultra-intense laser field. In its own rest frame, the highest energy electrons experience an electric field as high as one fifth of the critical field of QED. The experimental data can only be theoretically explained by taking into account radiation reaction occurring during the propagation of the electrons through the laser field consistently, as is the case with (semiclassical) Landau-Lifshitz and QED models. These results pave the way for the systematic study of strong radiation reaction in compact laser laboratories, an essential step towards the understanding of strong-field QED.

ACKNOWLEDGEMENTS:

G. Sarri wishes to acknowledge support from the Engineering and Physical Sciences Research Council (EPSRC), UK (grant numbers: EP/L013975 and EP/N022696/1). CPR, JMC and SPDM acknowledge support from EPSRC (grant numbers: EP/M018156/1 and EP/M018555/1). KP, JMC, EG, SPDM and ZN acknowledge funding from STFC (ST/J002062/1 and ST/P002021/1). AT and KB acknowledge support from the US NSF CAREER Award 1054164 and AT, KB, AJ and K.K from the US DOD under grant W911NF1610044. All the authors acknowledge the technical support from CLF.

REFERENCES:

-
- [1] L. D. Landau, and E. M. Lifshitz, The classical theory of fields (Elsevier, Oxford, 1975).
 - [2] A. Di Piazza *et al.*, “Extremely high-intensity laser interactions with fundamental quantum systems”, *Rev. Mod. Phys.* **84**, 1177 (2012) and references therein.
 - [3] M. Chen, E. Esarey, C. G. R. Geddes, C. B. Schroeder, G. R. Plateau, S. S. Bulanov, S. Rykovanov, and W. P. Leemans, “Modeling classical and quantum radiation from laser-plasma accelerators”, *Phys. Rev. ST Accel. Beams* **16**, 030701 (2013).

- [4] N. Neitz, A. Di Piazza, “Stochasticity Effects in Quantum Radiation Reaction”, *Phys. Rev. Lett.* **111**, 054802, (2013).
- [5] M. Vranic, T. Grismayer, R. A. Fonseca, and L. O. Silva, “Quantum radiation reaction in head-on laser-electron beam interaction”, *New J. Phys.* **18**, 073035 (2016).
- [6] V. Dinu, C. Harvey, A. Ilderton, M. Marklund, G. Torgrimsson, “Quantum Radiation Reaction: From Interference to Incoherence”, *Phys. Rev. Lett.* **116**, 044801 (2016).
- [7] V. S. Krivitskii, and V. N. Tsytovich, “Average radiation-reaction force in quantum electrodynamics”, *Sov. Phys. Usp.* **34**, 250 (1991).
- [8] V. B. Berestetskii, E. M. Lifshitz, and L. P. Pitaevskii, Quantum Electrodynamics (Elsevier Butterworth-Heinemann, Oxford, 1982).
- [9] V. I. Ritus, “Quantum effects of the interaction of elementary particles with an intense electromagnetic field”, *J. Russ. Laser Res.* **6**, 497 (1985).
- [10] J. Sultana, D. Kazanas, and A. Mastichiadis, “The supercritical pile gamma-ray burst model: The GRB afterglow steep-decline-and-plateau phase”, *Astrophys. J.* **779**, 16 (2013).
- [11] I. C. E. Turcu et al., “High field physics and QED experiments at ELI-NP”, *Romanian Reports in Physics*, **68** Supplement, S145 (2016).
- [12] J. P. Zou et al., “High Power Laser Science and Engineering Design and current progress of the Apollon 10 PW project”, *High Power Laser Science and Engineering* **3**, e2 (2015).
- [13] <http://spie.org/x103688.xml>
- [14] http://www.xcels.iapras.ru/2013_news.html
- [15] C. Bula et al., “Observation of Nonlinear Effects in Compton Scattering”, *Phys. Rev. Lett.* **76**, 3116 (1996).
- [16] D. L. Burke et al., “Positron Production in Multiphoton Light-by-Light Scattering”, *Phys. Rev. Lett.* **79**, 1626 (1997).
- [17] E. Esarey, C. Schroeder, and W. Leemans, “Physics of laser-driven plasma-based electron accelerators”, *Rev. Mod. Phys.* **81**, 1229 (2009) and references therein.
- [18] G. Sarri et al., “Ultrahigh Brilliance Multi-MeV Gamma-Ray Beams from Nonlinear Relativistic Thomson Scattering”, *Phys. Rev. Lett.* **113**, 224801 (2014).
- [19] K. Khrennikov et al., “Tunable All-Optical Quasimonochromatic Thomson X-Ray Source in the Nonlinear Regime”, *Phys. Rev. Lett.* **114**, 195003 (2015).

- [20] W. Yan *et al.*, “High-order multiphoton Thomson scattering”, *Nat. Phot.* published online: doi:10.1038/nphoton.2017.100
- [21] S. Kneip *et al.*, “Near-GeV Acceleration of Electrons by a Nonlinear Plasma Wave Driven by a Self-Guided Laser Pulse”, *Phys. Rev. Lett.* **103**, 035002 (2009)
- [22] K. Poder *et al.*, “Multi-GeV electron acceleration in strongly wakefields driven by oversized laser spots”, in preparation
- [23] G. M. Samarin, M. Zepf, and G. Sarri, “Radiation reaction studies in an all-optical set-up: experimental limitations” *J. Mod. Opt.* DOI: 10.1080/09500340.2017.1353655 (2017).
- [24] S. Corde *et al.*, “Femtosecond x rays from laser-plasma accelerators”, *Rev. Mod. Phys.* **85**,1 (2013).
- [25] A. Di Piazza, “Exact solution of the Landau-Lifshitz equation in a plane wave”, *Lett. Math. Phys.* **83**, 305 (2008).
- [26] A. G. R. Thomas, C. P. Ridgers, S. S. Bulanov, B. J. Griffin, and S. P. D. Mangles, “Strong Radiation-Damping Effects in a Gamma-Ray Source Generated by the Interaction of a High-Intensity Laser with a Wakefield-Accelerated Electron Beam”, *Phys. Rev. X* **2**, 041004 (2012).
- [27] G. Stupakov, and S. Heifets, “Beam instability and microbunching due to coherent synchrotron radiation”, *Phys. Rev. ST Accel. Beams* **5**, 054402 (2002).
- [28] J. G. Kirk, A. R. Bell, and I. Arka ”Pair production in counter-propagating laser beams”, *Plasma Phys. Contr. F.* **51**, 085008 (2009).
- [29] T. D. Arber *et al.*, “Contemporary particle-in-cell approach to laser-plasma modelling”, *Plasma Phys. Control. Fusion*, **57**, 113001 (2015).
- [30] A. Di Piazza, S. Meuren, M. Tamburini, and C. H. Keitel, “On the validity of the local constant field approximation in nonlinear Compton scattering”, arXiv:1708.08276 (2017).
- [31] S. Kneip *et al.*, “Bright spatially coherent synchrotron X-rays from a table-top source”, *Nat. Phys.* **6**, 980 (2010).
- [32] D. J. Corvan *et al.*, “Optical measurement of the temporal delay between two ultra-short and focussed laser pluses”, *Opt. Expr.* **24**, 3127 (2016).
- [33] C. Gregory, private communication.
- [34] H. D. Zhang *et al.*, “Beam halo imaging with a digital optical mask”, *Phys. Rev. ST-AB* **15**, 072803 (2012).

- [35] M. Tamburini *et al.*, “Radiation reaction effects on radiation pressure acceleration”, *New J. Phys.* **12**, 123005 (2010).
- [36] M. Tamburini, A. Di Piazza, C. H. Keitel, “Laser-pulse-shape control of seeded QED cascades”, *Sci. Rep.* **7**, 5694 (2017). See also arXiv:1511.03987 (2015).
- [37] C.P. Ridgers *et al.*, “Modelling Gamma Ray Emission and Pair Production in High-Intensity Laser-Matter Interactions”, *J. Comp. Phys.*, **260**, 273 (2014).

METHODS

Laser-wakefield accelerated electron beam: The electron beam was generated and accelerated during the propagation of an intense laser beam through a 2 cm long gas-cell filled with helium at a background pressure of 60 mbar that, once fully ionised, corresponds to an electron density of $2 \times 10^{18} \text{ cm}^{-3}$. The laser with a pulse duration of (42 ± 3) fs was focussed using an $f/40$ spherical mirror down to a focal spot with Full-Width-Half-Maxima (FWHM), along the two axis, of $\sigma_x = (59 \pm 2) \mu\text{m}$ and $\sigma_y = (67 \pm 2) \mu\text{m}$ containing 9 J (normalised intensity of $a_0 \approx 1.7$). Particle-In-Cell simulations of the electron acceleration indicate strong self-focussing of the laser in the plasma, resulting in a peak amplitude $\sqrt{a_0^f} \approx 3$. The laser beam accelerated electrons with a broad energy spectrum reaching approximately 2 GeV ($\gamma_e \approx 4 \times 10^3$). The electron beam source size can be estimated to be $D_e \leq 1 \mu\text{m}$, as deduced by rescaling the size of typical betatron sources in similar conditions [31]. The energy-dependent beam divergence was determined by measuring the beam width perpendicular to the direction of dispersion on the electron spectrometer screen 2 m downstream from the gas cell. For electron energies exceeding GeV, the divergence is measured to be $\theta_e = (1.0 \pm 0.2)$ mrad. Space charge effects appear to be negligible for electron energies exceeding 100 MeV, justifying the assumption of the electron beam divergence being constant throughout the propagation to the detector. Under this assumption the electron beam has, at the interaction point with the scattering laser (1 cm downstream of the exit of the gas-cell), a FWHM of $(11 \pm 2) \mu\text{m}$.

The scattering laser: one of the two laser beams (pulse duration of (42 ± 3) fs, energy after compression of (8.8 ± 0.7) J) of the Astra-Gemini system was focused, using an $f/2$ off-axis parabola with a concentric $f/7$ hole (energy loss of 10%), 1 cm downstream of the exit of the gas-cell. The Driver Laser and the Scattering Laser are generated from

the same oscillator and synchronised using a spectral interferometry technique discussed in Ref. [32] and already used in a similar experimental setup [18]. The system had a temporal resolution of approximately 40 fs. The radial distribution of the laser intensity at focus is shown in Fig. 1b. and it arises from an average of ten consecutive measurements at low power (spatial resolution of the detector of 0.2 $\mu\text{m}/\text{pixel}$). Independent measurements of the intensity profile at low-power and full-power indicate a broadening of the focal spot radius of the order of 10% in the latter case [33]. This effect is taken into account in the computed transverse laser field distribution shown in Fig. 1c.

The electrons are expected to be lagging behind the driver laser by approximately 75 fs, if we assume a bubble radius of $r_b \approx 2\sqrt{a_0^f}c/\omega_p \approx 23 \mu\text{m}$, with ω_p being the electron plasma frequency and $\sqrt{a_0^f} \simeq 3$ being the self-focussed vector potential [17, 22]. However, as the electrons are not injected at the beginning of the plasma there is an additional delay in electron beam arrival time associated with the laser pulse propagating in the plasma at its group velocity. This is of the order of tens of femtoseconds, depending on the exact injection point in the plasma. At this time delay, the scattering laser has a rather flat profile, with a peak a_0 of the order of 10 and a full width half maximum of 12 μm . Measurements of the pointing fluctuation of the laser-driven electron beam indicate, as an average over 100 consecutive shots, an approximately Gaussian distribution (confidence of 95% from the Kolmogorov-Smirnov test) centred on the laser propagation axis with a standard deviation of (3.2 ± 0.8) mrad [23].

The magnetic spectrometer: the magnetic spectrometer consisted of a 15 cm long dipole magnet with a peak magnetic field of 1.0 T. The magnet was placed 60 cm from the laser-electron interaction point and the dispersed electron beam was recorded by a LANEX scintillator screen placed 2 m away from the gas-cell. The screen was tilted by 45°, to improve spectral resolution. The minimum electron energy recorded on the LANEX screen in this configuration was 350 MeV. The LANEX screen was imaged in a Scheimplflug configuration [34], allowing the whole length of the screen to be in focus even at the 45° viewing angle. Given an electron beam divergence of $\theta_e = 1.0 \pm 0.2$ mrad, and a beam source size of $D_e \leq 1 \mu\text{m}$, the spectral resolution of the magnetic spectrometer can be estimated, for

ultra-relativistic electrons, as:

$$\frac{\delta E}{E} \approx \frac{(D_s + D_l)R\theta_s}{(D_l - L_m/2)L_m} \quad (2)$$

where D_l is the distance between the LANEX screen and the start of the magnet, L_m is the length of the magnet, R is the radius of curvature in the magnetic field for an electron of energy E , and D_s is the distance between the source and the start of the magnet. For an electron with an energy of $E = 1.5 \text{ GeV}$, $\delta E/E \approx 7\%$.

Multi-particle simulations: a beam of 10^7 electrons was generated by sampling from the experimental electron beam spectrum and energy-dependent divergence. First, the electron energy was sampled from the experimental electron spectrum. Second, for each orthogonal axis in the plane perpendicular to the propagation direction the divergence angle was independently sampled from a Gaussian distribution with mean zero and with FWHM given by the experimental electron energy-divergence function calculated at the previously sampled electron energy. Third, the electron three dimensional momentum was calculated from the sampled electron energy and from the two sampled divergence angles. In order to account for the free electron propagation from the gas-cell, the initial transverse electron spatial distribution was obtained assuming ballistic propagation of the electrons over 1 cm from a point-like source. The longitudinal electron distribution was assumed to be Gaussian with $12 \mu\text{m}$ FWHM, i.e. 40 fs duration. The transverse laser pulse field profile was obtained by fitting the experimental transverse profile (see Fig. 1b) with the linear superposition of two Gaussian pulses. Each Gaussian pulse was accurately modelled by including terms up to the fifth order in the diffraction angle. The resulting peak amplitude of the laser field at the focus was $a_0 \approx 22.5$ with approximately $2.5 \mu\text{m}$ FWHM of the transverse intensity profile. The laser pulse temporal profile was Gaussian with 42 fs duration FWHM of the laser pulse intensity. Since the accelerated electrons lag behind the laser pulse, the head-on collision between the peak of the scattering laser and the peak of the electron beam was set to occur 64 fs after the scattering laser pulse reached the focus. This results in both a reduction of the maximal laser field at the interaction from $a_0 \approx 22.5$ to $a_0 \approx 12.3$, and into an increased diameter (FWHM of the intensity) from $2.5 \mu\text{m}$ to about $6.9 \mu\text{m}$.

In order to account for shot-to-shot fluctuations of both lasers, simulations were performed with different initial electron spectra corresponding to a band within one standard deviation centred around the average spectrum. In addition, the amplitude of the scattering laser was also varied within a range of $\pm 5\%$, to account for the experimental uncertainty in the measured intensity. The theoretical uncertainty bands corresponding to the above-mentioned simulations are reported in Fig. 4a-d together with the experimental spectra. Four different sets of simulations were performed. In the first set of simulations electrons were evolved with the Lorentz force, and the corresponding Larmor emission energy was calculated during the evolution. In this perturbative approach, similarly to the one adopted in synchrotron machines, the total emitted energy was subtracted after the end of the laser-electron interaction (see Fig. 4a). In the second set of simulations electrons were evolved according to the reduced Landau-Lifshitz equation, i.e. the Landau-Lifshitz equation [1] where the small term containing the derivatives of the electromagnetic field is neglected [35] (see Fig. 4b). Note that, in addition to being negligibly small, the net effect of the terms containing the derivatives of the field average out at zero for a plane-wave pulse [25]. In the third set of simulations, a semiclassical model was employed, where energy losses are still modelled following the Landau-Lifshitz equation but with a correction factor multiplying the radiation reaction force, which takes into account that the classical theory overestimates the energy losses compared to the full QED theory. Finally, in the fourth set of simulations, a QED approach was employed, where stochastic photon emission was calculated for arbitrary electron and photon energy, and electrons were evolved according to the Lorentz equation between two consecutive photon emission events [36] (see Fig. 4d).

Particle-In-Cell simulations: Particle-in-cell (PIC) simulations were performed using the code EPOCH [29]. EPOCH uses the same model for radiation reaction as the QED model in the multi-particle simulations described above [37]. EPOCH also includes collective effects due to the charge and current in the electron beam; although the code assumes a charge neutralising background at the initial position of the electron beam in the simulation (thus overestimating the importance of collective effects in the case simulated here). Three dimensional EPOCH simulations were performed. The laser and electron bunch simulated were the same as in the multiparticle simulations. The spatial domain extended over $78.7 \mu\text{m}$

in the direction of laser propagation (discretised over 1020 cells) and 40 μm in each of the transverse directions (discretised over 920 cells). The collision between the laser pulse and electron bunch occurred 64 fs after the laser pulse reached focus. The electron bunch was represented by 1.5×10^7 macro-particles using third-order particle weighting. The data required to reproduce the PIC simulation results is available at [doi:10.15124/bd4a4a0b-78e3-405c-9318-1757b0209c54](https://doi.org/10.15124/bd4a4a0b-78e3-405c-9318-1757b0209c54).

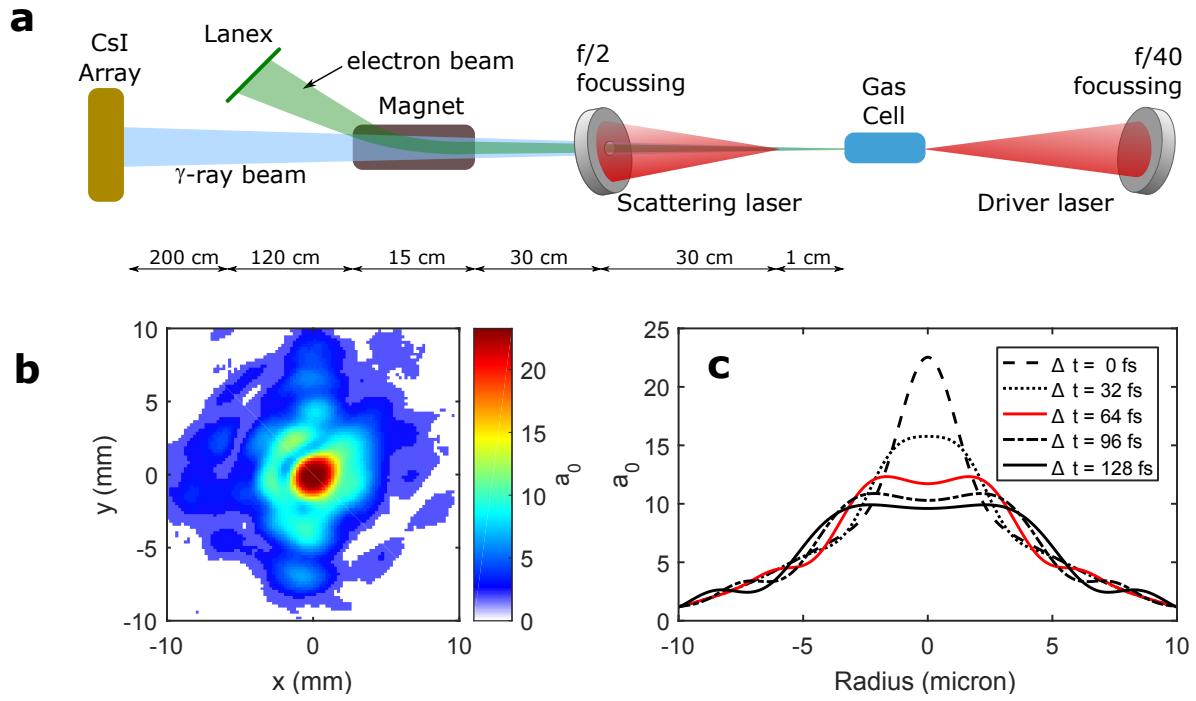


Figure 1. **Experimental setup:** **a.** Schematic of the experimental setup: details in the text. **b.** Typical measured spatial distribution of the intensity in focus of the Scattering Laser beam. **c.** Computed transverse distribution of the normalised laser field amplitude of the scattering laser at the overlap point as a function of delay between e-beam and scattering laser. Details in the methods section.

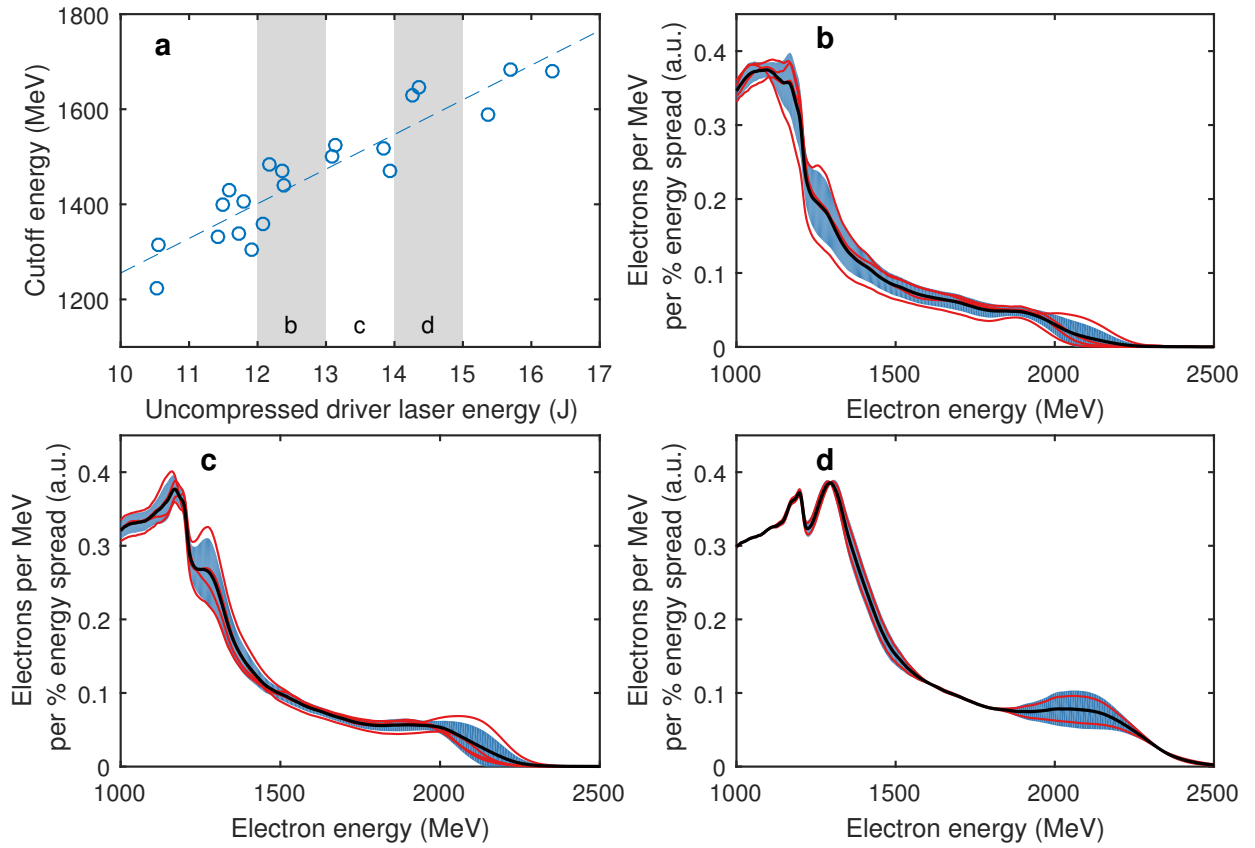


Figure 2. **Reference Electron Spectra:** **a.** Correlation between driving laser energy and the cut-off energy of the electron beam emerging from the accelerator (defined as the energy at which the number of electrons per MeV drops to 10% of the highest value at low energy). **b.** Electron spectra for a laser energy between 12 and 13 J. **c.** Electron spectra for a laser energy between 13 and 14 J. **d.** Electron spectra for a laser energy between 14 and 15 J. In frames b.-d., thin red lines represent single shots, thick black lines represent an average and the associated bands represent one standard deviation.

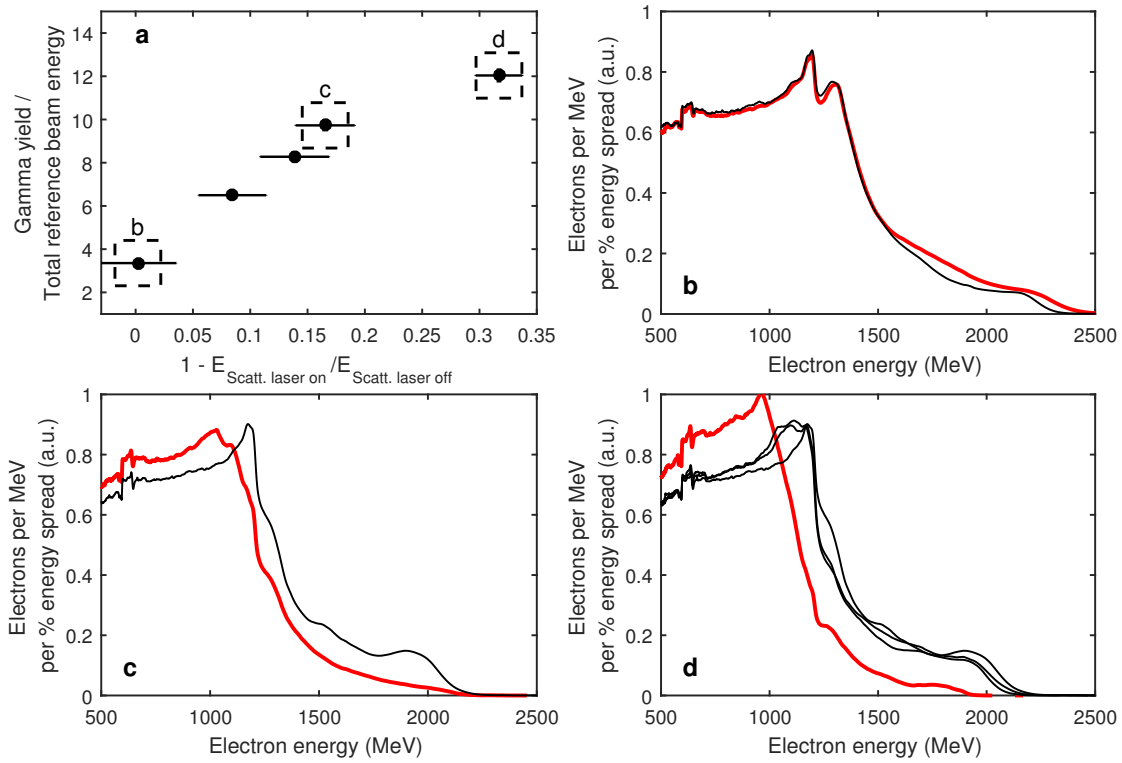


Figure 3. **Radiation Reaction Data:** **a.** Measured integrated γ -beam photon energy (normalised to the total kinetic energy in the un-scattered electron beam) versus amount of radiation friction experienced by the electron beam. Total friction is estimated by dividing the total kinetic energy in the scattered electron beam by the total kinetic energy in the related reference shot. **b.** - **d.** Measured electron spectrum after interaction with the scattering laser (thick red line) and related spectra with the scattering laser off (black thin line) for the three different scenarios shown in frame a.: poor overlap (frame b.), moderate overlap (frame c.), and best overlap (frame d.)

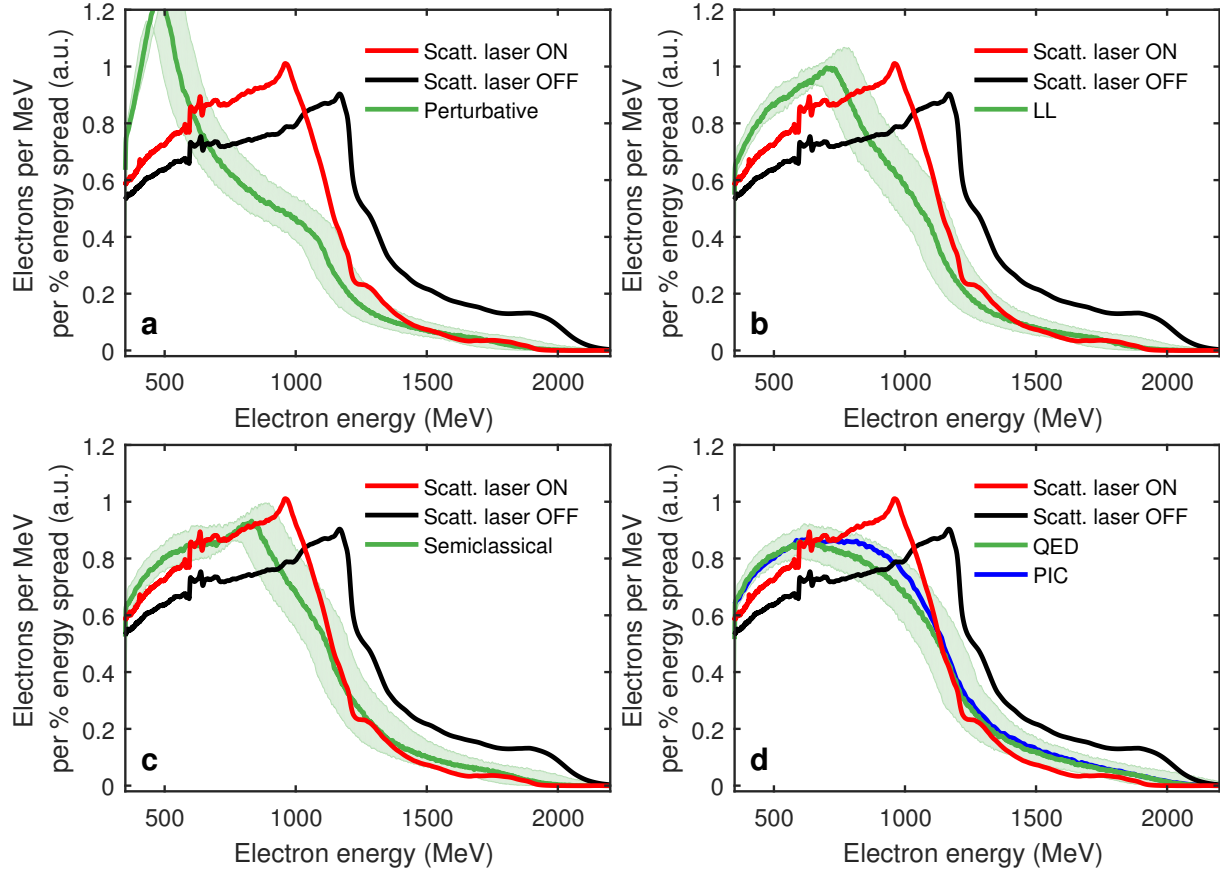


Figure 4. **Comparison of experimental results with theoretical models for the condition of best overlap:** The experimentally measured electron spectrum without the scattering laser (black line) and the spectrum of scattered electrons (red line) and **a.** the theoretical prediction assuming a model only based on the Lorentz force, **b.** the Landau-Lifshitz equation, **c.** a semiclassical model of radiation reaction and **d.** the quantum model of radiation reaction in a multi-particle code and in a PIC code (green and blue curves, respectively). In each frame, the uncertainties associated with the theoretical model arise from assuming the experimental uncertainty in the original electron spectrum, as arising from the energy uncertainty of the magnetic spectrometer, and shot-to-shot intensity fluctuations of the scattering laser. Details of the models used are discussed in the Methods section.